Synthesis of Conducting Polyaniline/TiO_2 Composite Nanofibres by One-step *In Situ* Polymerization Method

Chaoqing Bian, Yijun Yu, Gi Xue

Nanjing National Laboratory of Solid State Microstructure, Department of Polymer Science and Engineering, School of Chemistry and Chemical Engineering, Nanjing University, Nanjing 210093, China

Received 30 July 2006; accepted 2 October 2006
DOI 10.1002/app.25636
Published online 27 December 2006 in Wiley InterScience (www.interscience.wiley.com).

ABSTRACT: Conducting polyaniline (PANI)/titanium dioxide (TiO_2) composite nanofibres with an average diameter of 80–100 nm were prepared by one-step *in situ* polymerization method in the presence of anatase nano-TiO_2 particles, and were characterized via Fourier-transform infrared spectra, UV/vis spectra, wide-angle X-ray diffraction, thermogravimetric analysis, and transmission electron microscopy, as well as conductivity and cyclic voltammetry. The formation mechanism of PANI/TiO_2 composite nanofibres was also discussed. This composite contained ~ 65% conducting PANI by mass, with a conductivity of 1.42 S cm^{-1} at 25°C, and the conductivity of control PANI was 2.4 S cm^{-1} at 25°C. © 2006 Wiley Periodicals, Inc. J Appl Polym Sci 104: 21–26, 2007

Key words: polyaniline; nano-TiO_2; *in situ* polymerization; nanofibres; conductivity

INTRODUCTION

The discovery of conducting polymers has opened up a new promising field in material science and engineering. Among them, conducting polyaniline (PANI) is one of the most promising conducting polymers because of its unique electrical, optical, and optoelectrical properties, as well as its ease of preparation and excellent environmental stability. PANI can be used in electrochromic devices, light-emitting diodes, electrostatic discharge protection, secondary batteries, etc.[1–4] In recent years, one-dimensional PANI nanostructures, including nanowires, nanorods, and nanotubes, have been studied with the expectation that such materials will possess the advantages of both low-dimensional systems and organic conductors.[5–7] Especially, Zhang et al.[8] synthesized bulk quantities of doped PANI nanofibers in one step by the use of nanostructured seed templates, without the need for conventional templates, surfactants, polymers, or organic solvents. Nowadays, conducting PANI/inorganic nanocomposites have also attracted more and more attention. The properties of these nanocomposites are quite different from PANI and the corresponding inorganic nanoparticles due to interfacial interactions between inorganic nanoparticles and PANI macromolecules. And their properties can be easily adjusted to the desired applications via the variation of particle size, shape, and the distribution of nanoparticles. Consequently, they have many potential applications in electrical nanodevices.[9–17]

Among those inorganic nanoparticles, titanium dioxide (TiO_2) nanoparticles are appealing because of their excellent physical and chemical properties, as well as extensive applications in diverse areas, such as coatings, solar cells, and photocatalysts.[18–21] Many papers on PANI/TiO_2 nanocomposites have been published, but the morphology of most composite is the encapsulation of nano-TiO_2 particles inside the shell of conducting PANI. For instance, Feng et al.[22] synthesized a composite of PANI encapsulating nano-TiO_2 particles by *in situ* emulsion polymerization; Xia et al.[23] prepared PANI/nanocrystalline TiO_2 composite by ultrasonic irradiation; and Schnitzler et al.[24] obtained hybrid materials of nano-TiO_2 particles and PANI based on a sol–gel technique using titanium tetra-isopropoxide as oxide precursor. However, Zhang and coworkers' work was exceptional. They successfully synthesized PANI composites nanotubes with an average diameter of 90–130 nm through a self-assembly process in the presence of β-naphthalenesulfonic acid (β-NSA) as a dopant. And they found that PANI-β-NSA/TiO_2 composites were fibrous on condition that the concentration of nano-TiO_2 particles was lower than 0.08*M*.[25]

In this paper, we reported a simple method for the synthesis of conducting PANI/TiO_2 composite nanofibres, which could be easily applied industrially. PANI/TiO_2 composite nanofibres (80–100 nm in diameter) were prepared by one-step *in situ* polymerization of aniline in the presence of anatase nano-TiO_2 particles, and the concentration of nano-TiO_2 particles was

Correspondence to: G. Xue (xuegi@nju.edu.cn).
Contract grant sponsor: National Natural Science Foundation of China (NNSFC); contract grant numbers: 20374027, 50533020, 90403013.

Journal of Applied Polymer Science, Vol. 104, 21–26 (2007)

0.125*M* that was higher than 0.08*M*. The results of spectroanalysis illustrated that PANI and nano-TiO_2 particles were not simply blended in the composite. There was an interaction at the interface of PANI and nano-TiO_2 particles. It should be attributed to the tendency to form coordination compound between titanium and nitrogen atom in PANI macromolecular.[26] This composite contained $\sim$ 65% conducting PANI, and its conductivity was 1.42 S cm^{-1} at 25°C. It can potentially be used in charge storage and materials of solar cell because of its photovoltaic and absorption properties.

EXPERIMENTAL

Materials

Aniline (Shanghai Chemical Works, China) was distilled under reduced pressure. Nano-TiO_2 particles (anatase) with an average particle size of $\sim$ 20 nm (Jiang Su Hehai Nano-ST Company, China) were used as received. Other chemicals were also used as received without further purification. Water used in this study was deionized water.

Syntheses of PANI/TiO_2 composite nanofibres and control PANI

PANI/TiO_2 composite nanofibres were synthesized as follows: 1.8 mL aniline was injected into 70 mL of 2*M* HCl containing 1 g nano-TiO_2 particles under ultrasonic action to reduce the aggregation of nano-TiO_2 particles. After 12 h, 4.5 g $(NH_4)_2S_2O_8$ (dissolved in 20 mL deionized water) were dropped into solution with constant stirring. The polymerization was allowed to proceed for 5 h at 25°C. The precipitated powder was filtered under gravity, and washed with 2.0*M* HCl and deionized water, afterwards dried in a vacuum at 60°C for 24 h to obtain a fine tinted green powder.

Control PANI was prepared as above but without nano-TiO_2, and obtain a fine dark green powder.

Characterization

Fourier-transform infrared spectra (FTIR) of the powder samples were made with a fully computerized Bruker Vector22 spectrometer using KBr pressed discs.

UV/vis spectra of the samples, which were dispersed in deionized water under ultrasonic action, were recorded on a Perkin–Elmer Lambda35 UV/vis spectrophotometer.

Measurements of wide-angle X-ray diffraction (WXRD) were taken on a Shimadzu XD-3A instrument using a CuK_α radiation ($\lambda = 0.154$ nm).

Thermogravimetric analyses (TGA) were carried out on a Shimadzu TGA-50 instrument at a heating rate of 10°C min^{-1} in air.

The observations of the samples morphology were performed, using a JEM-100S transmission electron microscope (TEM) and a Hitachi X650 scanning electron microscope (SEM).

Conductivity measurements were made on compressed pellets of the powder using conventional four-point probe technique at ambient temperature (25°C).

Cyclic voltammetric studies of PANI and PANI/TiO_2 composite were performed with using a Model 273 polentiostat/golvanostat (EG and Princeton Applied Research). A one-compartment three-electrode cell was used with a platinum sheet as counter electrode and a saturated calomel electrode (SCE) as reference electrode. Electrolyte was 0.5*M* H_2SO_4. The scan speed was 50 mV s^{-1} and the potential range was from –200 to 1000 mV. To measure the cyclic voltammetry (CV), PANI or PANI/TiO_2 composite nanofibres (0.01 g) were suspended in 10 mL of deionized water and sonificated for 30 min. This suspension of several drops was carefully transferred to the surface of working electrode (gold sheet of 0.07 cm^2 surface area embedded in PTFE). After water evaporation (at room temperature) a uniform film was formed, then rinsed in ethanol.

RESULTS AND DISCUSSION

Morphology

TEM and SEM of nano-TiO_2 particles and PANI/TiO_2 composite are given in Figure 1. Figure 1(a) shows that the size of nano-TiO_2 particles was very uniform, but nano-TiO_2 particles were aggregated in aqueous solution due to their high surface energy. However, a different appearance was observed for the PANI/TiO_2 composite. Nanofibres with an average diameter of 80–100 nm were obtained as shown in Figures 1(b) and 1(c).

Because the nano-TiO_2 particles are electronegative in aqueous solution, anilinium cations can be adsorbed on the surface of nano-TiO_2 particles by the electrostatic attraction. Therefore, there are three components in this reaction system before adding $(NH_4)_2S_2O_8$, which are nano-TiO_2, free anilinium cations, and adsorbed anilinium cations on the surface of nano-TiO_2 particles. The formation of this composite should be the result that free aniline cation-radicals and adsorbed aniline cation-radicals on the surface of nano-TiO_2 particles grew together. Nano-TiO_2 particles were confined in the wall of the PANI/TiO_2 composite nanofibres because nano-TiO_2 particles were surrounded by anilinium cations during the formation of the composite nanofibres.

The formation of nanofibres can be explained by the anisotropy of growth rate. According to the classical theory of nucleation and growth, nanofibres are

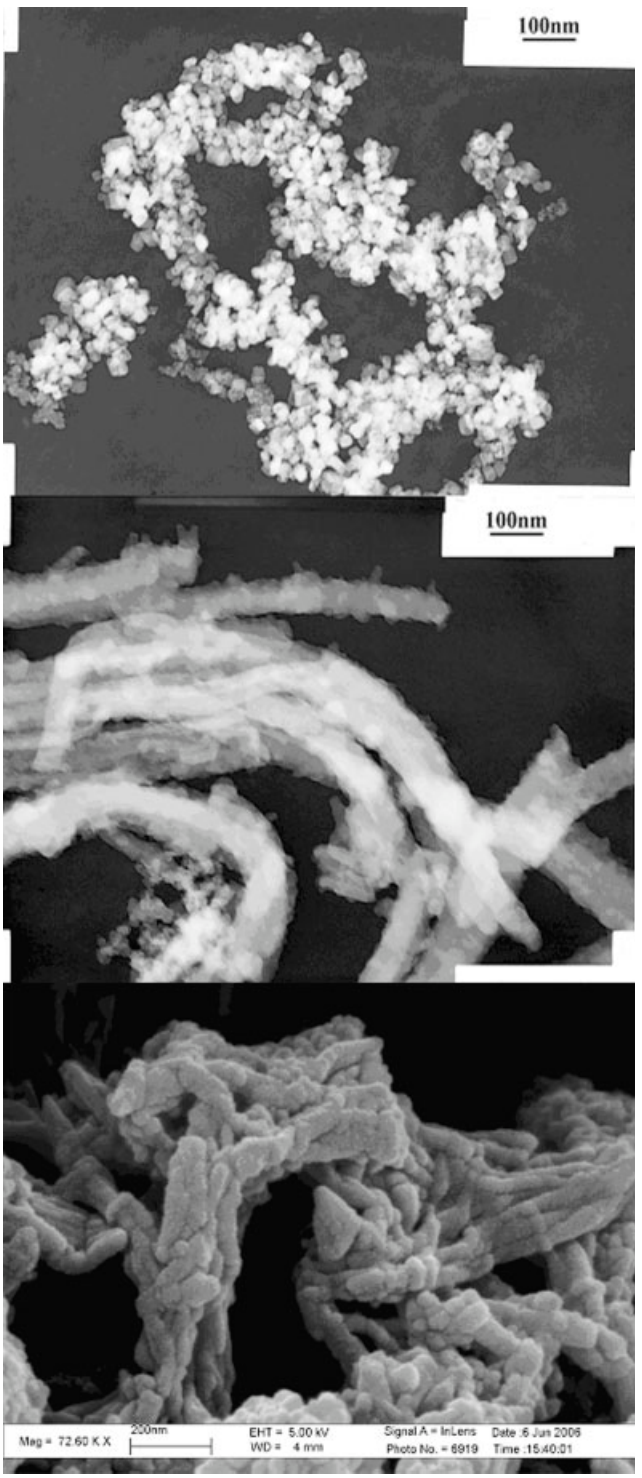

Figure 1 TEM and SEM of nano-TiO_2 and PANI/TiO_2 composite TEM of nano-TiO_2 (a), TEM of PANI/TiO_2 composite (b), and SEM of PANI/TiO_2 composite (c).

intrinsically formed in the initial stage of polymerization. In the early stages monomers and oxidants were depleted in the vicinity of the initially formed nanofibres. New reactive aniline cation-radicals and oligomers did not diffuse quickly enough to those nanofibres resulting in nanofibres surface surrounded by ''depleted solution'' (termed ''depletion region''). However, their ends extended to the ''less depleted regions.''[27,28] In these regions, the concentration of the reactive aniline cation-radicals and oligomers was higher than that in the ''depleted regions.'' Consequently, these nanofibres were able to continuously grow and elongate in one direction.

Fourier-transform infrared spectra

Figure 2 shows the FTIR spectra of PANI, nano-TiO_2, and PANI/TiO_2 composite, respectively. The characteristic peaks of PANI were assigned as follows: the peaks at 1565 and 1476 cm^{-1} were attributable to C=N and C=C stretching mode for the quinoid and benzenoid rings; the peaks at 1291 and 1234 cm^{-1} were attributed to C—N stretching mode for the benzenoid ring; while the peak at 1117 cm^{-1}, which was formed during protonation, was assigned to a in-plane bending vibration of C—H.[29] Figure 2(b) indicates that the main characteristic peaks of PANI appeared in FTIR spectra of PANI/TiO_2 composite. And the presence of nano-TiO_2 particles led to the shift of some peaks in PANI macromolecules or the changes of relative intensity. In particular, the peaks at 1476 and 1291 cm^{-1} shifted to higher wavenumbers, corresponding to the stretching mode of C=C and C—N. In addition, the peak associating with the doping of PANI also shifted from 1117 to 1133 cm^{-1}. These obvious changes suggested that an interaction existed between nano-TiO_2 particles and PANI because titanium is a transition metal and titanic has intense tendency to form coordination compound with nitrogen atom in PANI macromolecular.[26]

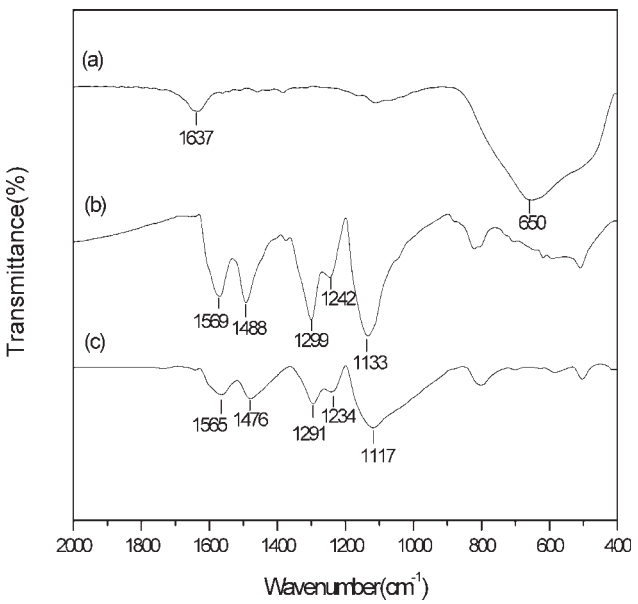

Figure 2 FTIR spectra of nano-TiO_2 (a), PANI/TiO_2 composite (b), and PANI (c).

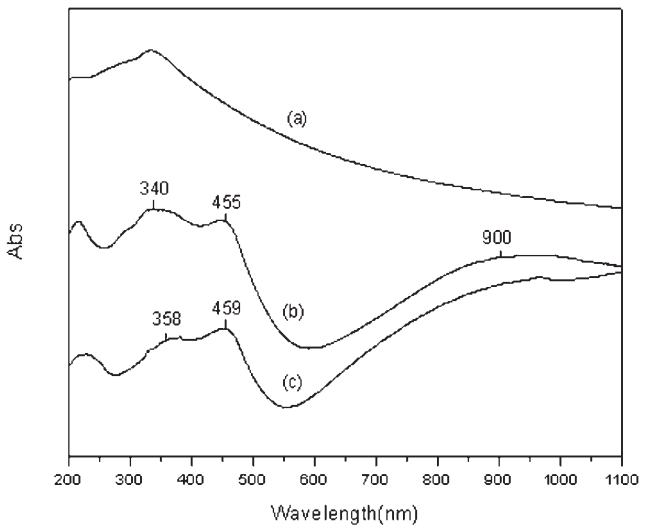

Figure 3 UV/vis spectra of nano-TiO_2 (a), PANI/TiO_2 composite (b), and PANI (c).

UV/vis spectra

UV/vis spectra of nano-TiO_2, PANI/TiO_2 composite, and PANI are provided in Figure 3.

Figure 3(c) clearly indicates that PANI had three characteristic peaks, which were at about 358, 459, and over 1100 nm. The peak at 358 nm arises from electron transition within the benzenoid segments, while the absorption peaks at 459 nm and over 1100 nm originates from the charged cationic species known as polarons.[25] From Figure 3(b), it was noted that the characteristic peaks of nano-TiO_2 and PANI all appeared in the UV/vis spectrum of PANI/TiO_2 composite. However, the peak at over 1100 nm obviously shifted to about 900 nm, and the relative intensity of these peaks was also changed. These changes should be attributable to the presence of nano-TiO_2. The interaction between nano-TiO_2 and PANI decreases the degree of orbital overlapping between π electrons of phenyl rings with the lone pair of nitrogen atom. Consequently, the extent of conjugation of PANI diminishes,[30] as a result the peaks occurred shift. Figure 3(c) shows that control PANI had a higher concentration of polaron than PANI/TiO_2 composite. This suggested that the presence of nano-TiO_2 also affected the doping level of PANI.

Wide-angle X-ray diffraction

Figure 4 gives WXRD patterns of the nano-TiO_2, PANI/TiO_2 composite, and PANI. Figure 4(c) suggests that the doped PANI was partly amorphous and partly crystalline. A peak, which was about 25° for PANI, should be assigned to the scattering from the periodicity perpendicular to PANI chains.[22,31,32] Although the PANI/TiO_2 composite contained 65% PANI, the peak of PANI did not show up in the WXRD pattern of PANI/TiO_2 composite, as shown in Figure 4(b). This indicated that the most of PANI were deposited on the surface of nano-TiO_2 particles and the presence of nano-TiO_2 particles influenced the crystallinity of PANI. Therefore, the broad weak diffraction peaks of PANI disappear.

Thermogravimetric analysis

Figure 5 illustrates the thermogravimetric curves of PANI and PANI/TiO_2 composites. Nano-TiO_2

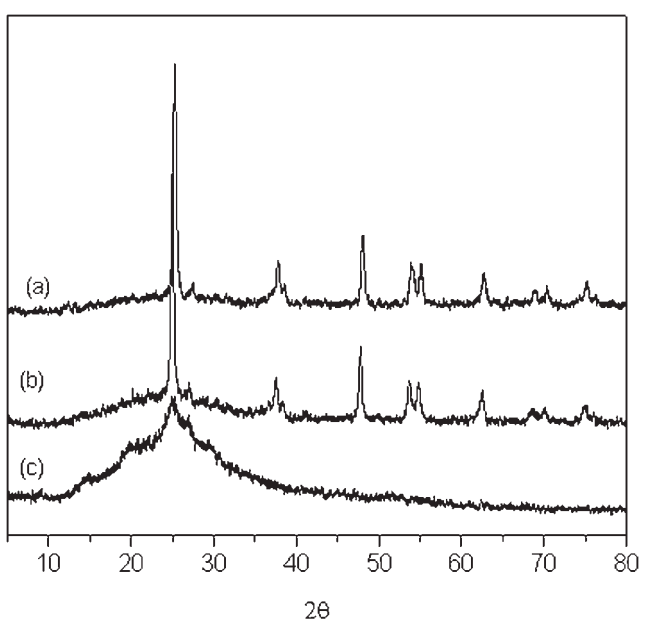

Figure 4 WXRD of nano-TiO_2 (a), PANI/TiO_2 composite (b), and PANI (c).

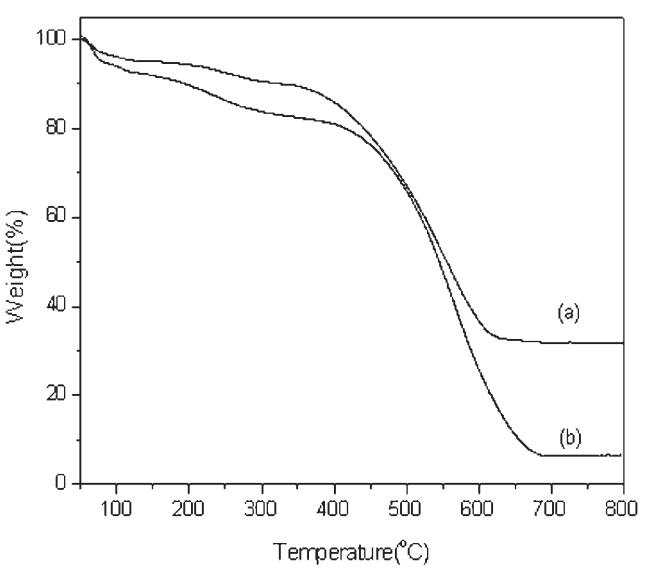

Figure 5 Thermogravimetric curves of PANI/TiO_2 composite (a) and PANI (b).

particles were very stable in air and almost no decomposition took place in the range of 20–800°C.[26] Figure 5(b) reveals that the sharp weight loss for PANI began at nearly 120°C, and continued until at 700°C. This should be due to the thermal degradation of PANI chains on a large scale. The thermal decomposition temperature of PANI was ~ 420°C in PANI/TiO_2 composite, which was lower than that of control PANI (~ 465°C). It was highly likely that the lower temperature was associated with the effect of nano-TiO_2 particles upon PANI macromolecules. The coordination between titanium and nitrogen atom probably weakened the interaction of interchains in PANI macromolecules, and helped the thermal degradation of PANI. The mass percentage of PANI layer in this composite was 65% in comparison with Curve-a and Curve-b in Figure 5.

Conductivity

Although the presence of nano-TiO_2 particles had an effect on the doping of PANI, the conductivity of this composite still reached 1.42 S cm^{-1} at 25°C, which was close to that of control PANI (2.4 S cm^{-1} at 25°C). This should be attributable to the more ordered arrangement of PANI in the composite.

Cyclic voltammetry

CV of PANI and PANI/TiO_2 composite was performed in 0.5*M* H_2SO_4 electrolyte and sample CVs are shown in Figure 6. From Figure 6(a), it was seen that PANI coatings deposited on the gold electrodes showed three pair redox processes, which were related to the typical interconversion reaction of PANI upon varying the potential. The first oxidation wave peak in the CV (at E_{SCE} = 211 mV) had maximum peak current, which was assigned to the leucoemeraldine to emeraldine transition, and the oxidation wave at around E_{SCE} = 695 mV was due to the transition from the emeraldine to the pernigraniline state. Between this two main pairs of peaks, a small definition peak located at E_{SCE} = 507 mV was seen, which correspond to the degradation products of PANI film.[33,34] During 50 cycles, the oxidation wave at E_{SCE} = 211 mV shifted to the more positive potentials and the peak current tardily decrease, and the current density of the oxidation wave at E_{SCE} = 507 mV gradually increased, indicating the electrochemical degradation of PANI film. Figure 6(b) suggests that electroactivity of PANI/TiO_2 composite was from the layer of conducting PANI. And CV of PANI/TiO_2 composite was similar to that of PANI during 10 cycles, except that two redox pair characteristics shifted from 211 and 695 mV to 231 and 771 mV. However, after 50 cycles the oxidation wave peaks at E_{SCE} = 771 mV and E_{SCE} = 507 mV gradually disappeared,

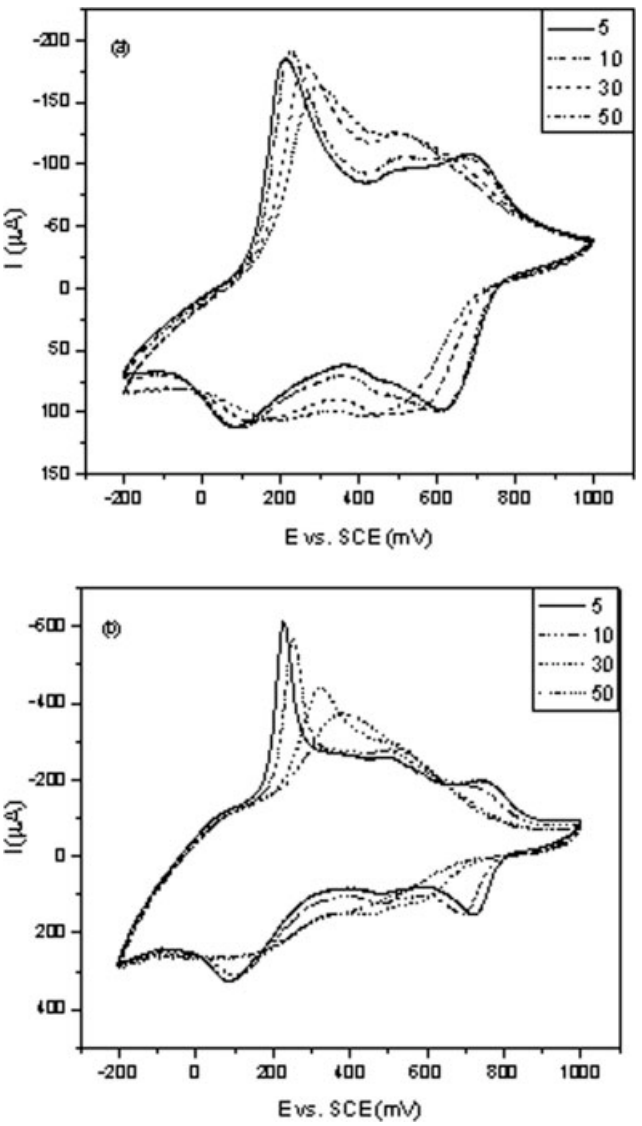

Figure 6 Cyclic voltammorgrams of PANI (a) and PANI/TiO_2 composite (b). Electrolytic solution: 0.5*M* H_2SO_4; sweep rate: 50 mV s^{-1}.

while the oxidation wave peak at E_{SCE} = 231 mV also shifted to the more positive potentials and the peak current obviously decrease. This meant that the presence of nano-TiO_2 particles accelerated the electrochemical degradation of PANI film, and debased the redox reversibility of PANI/TiO_2 composite. This behavior should also be attributable to the interaction existed between PANI and nano-TiO_2.[24]

CONCLUSIONS

Conducting PANI/TiO_2 composite nanofibres were prepared by one-step *in situ* polymerization of aniline in the presence of anatase nano-TiO_2 particles. The diameters of nanofibres were 80–100 nm, and its conductivity was 1.42 S cm^{-1} at 25°C. Because of the

tendency to form coordination compound between titanium and nitrogen atom in PANI macromolecular, PANI and nano-TiO_2 particles were not simply blended in this composite. An interaction existed between nano-TiO_2 particles and PANI macromolecule. The method we employed is very simple and inexpensive, and it can be easily applied industrially.

References

1. Gospodinova, N.; Terlemezyan, L. Prog Polym Sci 1998, 23, 1443.
2. MacDiarmid, A. G. Angew Chem Int Ed 2001, 40, 2581.
3. Huang, J. X.; Virji, S.; Weiller, B. H.; Kaner, R. B. J Am Chem Soc 2003, 125, 314.
4. Virji, S.; Huang, J. X.; Kaner, R. B.; Weiller, B. H. Nano Lett 2004, 4, 491.
5. Wang, D. Y.; Caruso, F. Adv Mater 2001, 13, 350.
6. Huang, J. X.; Kaner, R. B. Angew Chem Int Ed 2004, 116, 5941.
7. Huang, J. X.; Virji, S.; Weiller, B. H.; Kaner, R. B. Chem Eur J 2004, 10, 1314.
8. Zhang, X. Y.; Goux, W. J.; Manohar, S. K. J Am Chem Soc 2004, 126, 4502.
9. Gangopadhyay R.; De A. Chem Mater 2000, 12, 608.
10. Kim, B. H.; Jung, J. H.; Hong, S. H.; Kim, J. W.; Choi, H. J.; Joo, J. Curr Appl Phys 2001, 1, 112.
11. Liu, H.; Wang, J. Y.; Hu, X. B.; Robert, I. B.; Zhao, S. R.; Li, Q.; Jiang, M. H. Chem Phys Lett 2002, 352, 185.
12. Deng, J. G.; Ding, X. B.; Zhang, W. C.; Peng, Y. X.; Wang, J. H.; Long, X. P.; Li, P; Chan, A. S. C. Polymer 2002, 43, 2179.
13. Park, N. G.; Ryu, K. S.; Park, Y. J.; Kang, M. G.; Kim, D. K.; Kang, S. G.; Kim, K. M.; Chang, S. H. J Power Sources 2002, 103, 273.
14. Schnitzler, D. C.; Meruvia, M. S.; Hümmelgen, I. A.; Zarbin, A. J. G. Chem Mater 2003, 15, 4658.
15. Yu, Y. J.; Che, B.; Si, Z. H.; Li, L.; Chen, W.; Xue, G. Synth Met 2005, 150, 271.
16. Zhang, L. J.; Wan, M. X.; Wei, Y. Synth Met 2005, 151, 1.
17. Lee, C. F.; Tsai, H. H.; Wang, L. Y.; Chen, C. F.; Chiu, W. Y. J Polym Sci Part A: Polym Chem 2005, 43, 342.
18. O'Regan, B.; Gratzel, M. Nature 1991, 353, 737.
19. Norimoto, M. K.; Watanabe, T.; Hashimoto, K.; Fujishima, A. J Mater Sci 1999, 34, 2569.
20. Liu, X. H.; Liang, C. X.; Wang, H. Z.; Yang, X. J.; Lu, L. D.; Wang, X. Mat Sci Eng A 2002, 326, 235.
21. Chowdhury, D.; Palu, A.; Chattopadhyay, A. Langmuir 2005, 21, 4123.
22. Feng, W.; Sun, E.; Fujii, A.; Wu, H. C.; Niihara, K.; Yoshino, K. Bull Chem Soc Jpn 2000, 73, 2627.
23. Xia, H. S.; Wang, Q. Chem Mater 2002, 14, 2158.
24. Schnitzler, D. C.; Zarbin, A. J. Z. G. J Bruz Chem Soc 2004, 15, 378.
25. Zhang, L. J; Wan, M. X. J Phys Chem B 2003, 107, 6748.
26. Li, X. W.; Chen, W.; Bian, C. Q.; He, J. B.; Xu, N.; Xue, G. Appl Surf Sci 2003, 217, 16.
27. Bunker, B. C.; Rieke, P. C.; Tarasevic, B. J.; Campbell, A. A.; Gryxell, G. E.; Graff, G. L.; Song, L.; Virden, J. W.; Mcvay, G. L. Science 1994, 264, 48.
28. Chiou, N. R.; Epstein, A. J. Synthetic Metals 2005, 153, 69.
29. Kang, E. T.; Neho, K. G.; Tan, K. L. Prog Polym Sci 1998, 23, 277.
30. Schemid, A. L.; Cóordoba de Torrest S. I.; Bassetto, A. N.; Carios, I. A. J Braze Chem Soc 2000, 11, 317.
31. Zhang, L. J.; Wan, M. X. Adv Funct Mater 2003, 13, 815.
32. Cheng, F. G.; Tang, W.; Li, C. S.; Chen, J.; Liu, H. K.; Shen, P. W. Chem Eur J 2006, 12, 3082.
33. Arsov, L. J.; Plieth, W.; Koβmehl, G. J Solid State Electrochem 1998, 2, 355.
34. Shreepathi, S.; Holze, R. Chem Mater 2005, 17, 4078.